Fracture and Weakening of Jammed Subduction Shear Zones, Leading to the Generation of Slow Slip Events

Adam Beall[1], Åke Fagereng[1] and Susan Ellis[2]

[1]School of Earth and Ocean Sciences, Cardiff University, Cardiff, UK

[2]GNS Science, Avalon, Lower Hutt, New Zealand

Key Points:

- Fracturing of strong clasts in a weak mélange occurs at applied stresses 80% lower than for a homogeneous fault
- Fracturing of clasts in load-bearing force chains leads to stress redistribution into the viscously creeping matrix
- Clast strength must be reduced significantly in order to generate transient slip, depending on the degree of mélange jamming

Corresponding author: Adam Beall, bealla1@cardiff.ac.uk

This article has been accepted for publication and undergone full peer review but has not been through the copyediting, typesetting, pagination and proofreading process which may lead to differences between this version and the Version of Record. Please cite this article as doi: 10.1029/2019GC008481

Abstract

Geodetic data have revealed that parts of subduction interfaces creep steadily or transiently. Transient slow slip events (SSEs) are typically interpreted as aseismic frictional sliding. However, SSEs may also occur via mixed visco-brittle deformation, as observed in shear zones containing mixtures (mélange) of strong fractured clasts embedded in a weak visco-brittle matrix. We test the hypothesis that creep in a subduction mélange occurs through distributed matrix deformation, where flow is intermittently impeded by load-bearing clast networks (jamming). Our numerical models demonstrate that bulk mélange rheology can be dominated by the strong clasts in the absence of fracturing, while at high driving stresses or low frictional strength, clast fracturing redistributes deformation into the matrix, leading to high bulk strain-rates. Because mélange stress is heterogeneous, fracturing of clasts occurs throughout jammed mélange when the driving stresses are only $\sim 20\%$ of the clast yield strength. The effective rheology of jammed mélange can be characterised by a logarithmic dependence of stress on strain-rate, which is used to explore strain-rate transients caused by temporal variation in clast friction. Clasts must weaken significantly ($\sim 75\%$) in order to increase strain-rate by $8\times$. Spring-block slider models with a more idealized visco-brittle rheology also demonstrate that strain-rate transients can be generated when rate-and-state friction is incorporated. We outline a model where high bulk strain-rates are generated when pervasive fracturing occurs, but further slip is limited by viscous processes. Incorporating such viscous damping into models may widen the conditions under which SSEs can occur while preventing development of seismic slip.

Plain Language Summary

While some subduction zones are responsible for generating large earthquakes, others creep steadily or episodically. This range of deformation styles may correspond to the interplay between viscous creep and frictional failure, as observed in exhumed subduction shear zones, which are typically mixtures (mélanges) of strong fractured and weak viscous materials. We use computer models to explore how mélange strength and deformation style varies when the frictional material fractures. Load-bearing networks of unfractured strong material contribute significantly to mélange strength, so the onset of fracturing redistributes some deformation into the weak viscous material. As the force distribution in these networks is complicated, the onset of frictional failure alone is in-

sufficient to completely unload the strong material. However, if the frictional material weakens considerably, mélange may undergo a period of rapid, predominately viscous deformation. Cycles of viscous deformation may correspond to episodic creep events. If creep events do occur primarily by a viscous mechanism, this may explain why they can occur routinely in some regions without transitioning to seismic slip.

1 Introduction

The rheology and frictional properties of the subduction thrust interface exert a first-order control on the generation of major earthquakes (Scholz, 1998; van Dinther et al., 2013) and the maximum sustainable stresses and deformation rates at a convergent margin (Duarte et al., 2015; Behr & Becker, 2018). The down-dip limit of a subduction thrust seismogenic zone is often thought to be limited by the onset of steady viscous creep at temperatures $>350^{o}$C (e.g. Hyndman et al., 1997). Slow slip events (SSEs), episodes of aseismic slip rates of $\sim$0.1 - 1 m/year (faster than plate velocities) and commonly associated with tectonic tremor, have been observed in this transition zone (Rogers & Dragert, 2003; Schwartz & Rokosky, 2007). These events require an evolution in our understanding of the gradual spatial transition between the seismogenic zone and deeper, steady aseismic creep. SSEs have been primarily considered to arise due to frictional dynamics (Liu & Rice, 2005; Leeman et al., 2018). It has also been proposed that SSEs can result from dynamic interaction between viscous and frictional deformation (Ando et al., 2012; Fagereng et al., 2014; Hayman & Lavier, 2014), though it is still unclear which visco-brittle rheological model is most appropriate.

Mélange, a mixture of strong clasts embedded in a weak matrix, is commonly found in exhumed subduction-related shear zones and in some places preserves a mixture of contemporaneously developed brittle and ductile structures resulting from the interplay between relatively strong (brittle) clasts and weak (ductile) matrix (Fagereng & Sibson, 2010). Matrix deformation is typically distributed, likely resulting from predominately ductile processes such as pressure solution, observed at the μm scale in fine-grained quartz and calcite in combination with dilation of phyllosilicate cleavage (Bos & Spiers, 2001; Kitamura et al., 2005; Rowe et al., 2011; Wassmann & Stöckhert, 2013; Fagereng & den Hartog, 2016). Such pressure solution may be responsible for subduction interface creep. Fractures, predominately found in clasts, are indicative of locally elevated strength and stress (in the absence of extreme pore pressure variation). Depending on the connectiv-

ity of these higher stress clasts, there may be no connected matrix pathways for simple shear to occur, in which case the mélange rheology will be strong (referred to as jammed) and dependent on clast fracturing. Such load-bearing networks are called force chains and their reorganisation is responsible for stick-slip events in granular materials (Hayman et al., 2011). As a result of force chain dynamics, viscous and brittle deformation observed in exhumed mélanges may preserve cycles of alternating deformation mechanisms, perhaps generating SSEs.

Viscous creep can stabilise sliding of frictional minerals (Niemeijer, 2018), producing velocity-strengthening behaviour. Velocity-strengthening parts of a subduction interface can produce an SSE by damping an otherwise unstable rupture initiating in velocity-weakening material (Skarbek et al., 2012; Luo & Ampuero, 2018). Analogue models show that slow stick-slip events can occur in a macroscopically homogeneous viscoplastic material likely due to reorganisation of microgel force chains (Reber et al., 2015; Birren & Reber, 2019). These analogue models showed that microscopically these events are related to reorganisation of force chains, while macroscopically they correspond to episodic opening of tensile fractures, which grade into shear fractures and viscous deformation accommodating overall simple shear. In contrast, slow stick-slip events have been produced in rock experiments at normal stresses of < 10 MPa and high (>0.9) apparatus to critical stiffness ratios (Kaproth & Marone, 2013; Scuderi et al., 2017; Leeman et al., 2018). Visco-brittle interactions are difficult to quantify in such experiments, but microstructural observations indicate that frictional instabilities occur when deformation localizes in shear bands, and slip style may be controlled by the interplay between the rheology of shear bands and the surrounding fault rock (Scuderi et al., 2017). It is, however, still unclear if ductile and brittle interactions are necessary to produce strain-rate transients such as SSEs, and if rheological interactions do occur, what are the fundamental processes and scales at which they operate.

Finite element models demonstrate that minor shear strain of mélange with around 50% or more relatively competent material leads to the formation of clast force chains that block matrix pathways (Fig. 1a), switch the mélange to clast-dominated deformation (jamming), and consequently decrease bulk strain-rate by more than an order of magnitude (Webber et al., 2018; Beall et al., 2019). We explore the hypothesis that force chains may be disabled through the fracturing of clasts as their yield strength is reached after jamming (Fig. 1b), redistributing stress into the matrix and increasing bulk shear zone

strain-rate. If this hypothesis is correct, mélange deformation could temporarily switch between being limited by frictional failure and being controlled by viscous creep, as proposed in previous models (Lavier et al., 2013; Reber et al., 2015). Geological evidence for such visco-brittle interaction indicates this process could occur from centimetre up to 100s of metre scales (Fagereng & Sibson, 2010; Fagereng, 2011a; Rowe et al., 2011; Grigull et al., 2012; Hayman & Lavier, 2014). To integrate such frictional-viscous shear zone dynamics into large scale models, mélange deformation must be parameterized into a bulk rheology relating effective stresses to strain-rates.

Mélange clasts are commonly fractured, despite the low differential stress implied by creep of adjacent matrix. This fracturing is typically thought to indicate near-lithostatic pore-pressure (e.g. Sibson, 1996). However, stress within clasts is likely to be higher than the bulk applied stress, for isolated clasts (Schmid & Podladchikov, 2003) and more-so for load-bearing frameworks (Handy, 1994). Beall et al. (2019) showed that the shear stress of clasts within a subduction zone mélange can be increased by $> 3\times$ for unjammed mélange and $< 14\times$ in jammed mélange, which may drive fracture at lower pore-pressure. These models did not incorporate fracturing, so it is unclear how pervasive fracturing would be and how it would affect mélange rheology. In this study, we incorporate fracturing into our numerical mélange models and quantify both 1) how pervasive clast fracturing is at varying shear zone stress, and 2) whether fracturing could effectively disable force chains and increase shear zone strain-rates.

2 Bulk Rheology of a Subduction Interface: Theoretical Mixture Model Predictions

Geodynamic models of visco-brittle subduction interface deformation typically combine one viscous and one brittle rheology into a composite rheology (Karato, 2012), following the assumption that both rheologies experience either the same stress (iso-stress, the Reuss model) or the same strain (iso-strain, the Voigt model). The choice of Reuss or Voigt model dictates which rheology dominates at low and high stress (Fig. 1c).

The Reuss model represents material that can always viscously flow (though slowly for high viscosities), but switch to frictional deformation if a yield stress is reached. For predominately viscous slip transients to occur in a Reuss mixture, the viscous rheology must be highly non-linear (e.g. incorporating shear heating; Goswami & Barbot, 2018). The Voigt model, which is equivalent to a Bingham plastic when one of the materials

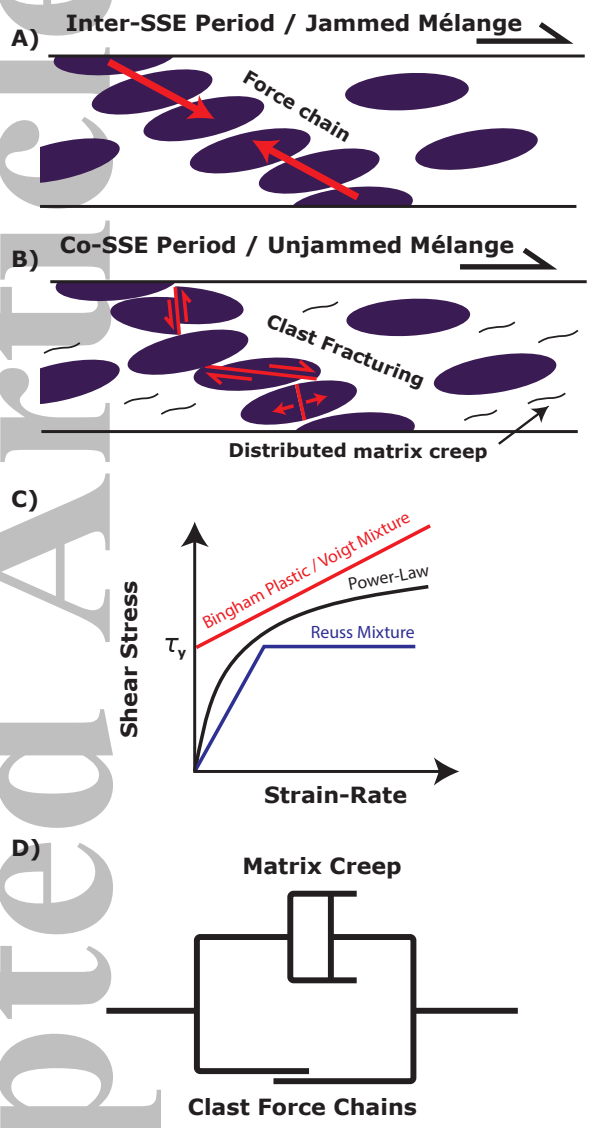

Figure 1. A) Periods of negligible megathrust creep in-between SSEs are hypothesised to be due to the formation of clast force chains, which prevent viscous matrix deformation. B) Clast fracture may redistribute stress into the weak matrix, switching the mélange to predominately viscous deformation with an associated increase in strain-rate. C) Schematic comparison of the Voigt (equivalent to Bingham plastic) and Reuss mixture models, and comparison to power-law rheology. When fracturing begins at $\tau = \tau_y$ (or lower if local stress amplification is considered), the Voigt model is rate-limited by viscous deformation, while the Reuss model becomes stress-limited by frictional deformation (which may be modestly rate-strengthening or weakening, or constant as shown here). D) We hypothesise that the rheology of a jammed mélange can be modelled as a viscous dashpot (matrix creep) in parallel with a frictional slider (fracture of clasts, neglecting their slow viscous creep), equivalent to a Bingham plastic.

Table 1. Symbols commonly used (spring-block slider model parameters in lower section)

Parameter	Symbol	Value
Average top boundary shear-stress	τ_b	-
Effective shear-strain-rate	$\dot{\gamma}_b$	-
Effective shear-strain	γ	-
Boundary velocity, average	V, V_{av}	-
Max., min. principal deviatoric stresses	σ_1, σ_2	-
Average dynamic normal stress	p	-
Shear stress (maximum)	τ	-
Shear strain-rate (maximum)	$\dot{\gamma}$	-
Yield stress (variable or constant)	τ_y	$\approx$ 21 - 160 MPa
Friction coefficient	μ	0.7 or 0
Cohesion	C	-
Overburden thickness	z	40 km
Tensile strength	T	-
Power-law rheology exponent	n	-
Fitting constants	c_0, c_1	-
Volumetric clast proportion	ϕ	0.35 - 0.61
Matrix viscosity	η_m	-
Clast viscosity	η_c	$10^3\eta_m$
Effective frictional viscosity	η_f	-
Pore-pressure ratio	λ	0.8
Effective normal stress	σ_{eff}	$\approx$ 208 MPa
Model height (shear-zone thickness)	L	100 m or 50 m
Ratio of clast short-axis length to L	D	0.05 - 0.28
Maximum D	D_{max}	0.14 - 0.28
Non-dimensionalised τ_b	τ_b'	τ_b/τ_y
Non-dimensionalised $\dot{\gamma}_b$	γ_b'	$\dot{\gamma}_b\eta_m/\tau_y$
Lower, upper yield stresses	τ_{y1}, τ_{y1}	-
Lower, upper stress thresholds	τ_0, τ_1	-
Critical viscosity	η_{mc}	-
Spring constant	k	10^8 Pa / m
Subduction velocity	V_p	10^{-9} m/s
Rate-and-state parameters	μ_0, a, b, θ, V_0, D_c	-

is frictional (Fig. 1c), represents a material that does not deform at all until frictional sliding occurs, at which point viscous deformation becomes rate-limiting and a low viscosity may produce high strain-rates (used by Ando et al., 2012; Lavier et al., 2013). Stress-dependent viscous deformation is generally captured by the power-law rheology $\dot{\gamma} \propto \tau^n$ (Fig. 1c) for maximum shear strain-rate $\dot{\gamma}$ and stress τ (we express stress throughout as maximum shear-stress, which is 50% of differential stress; Karato, 2012). The magnitude of the stress exponent n dictates how stress-dependent the rheology is, for example $n \approx 3$ for dislocation creep and $n \to \infty$ for a plastic material with a yield strength. It is unclear which model best captures the rheology of a subduction interface shear zone.

If a mélange only deforms when clasts in a force chain can deform, then assuming that clast and matrix strain is equal will give the Voigt / Bingham model. This model predicts negligible strain during time periods between SSEs, which is supported by GPS records, that generally show strong inter-SSE locking on interface patches hosting SSEs (Dragert et al., 2001; Wallace & Beavan, 2010; Li et al., 2016).

The bulk stress τ_b of a Voigt mixture with homogeneous clast stress τ_{clast} and matrix stress τ_{matrix} is calculated as $\tau_b = \phi\tau_{clast} + (1-\phi)\tau_{matrix}$. If clasts are purely frictional, τ_{clast} is limited to a yield stress τ_y, and if τ_{matrix} is controlled by Newtonian viscous creep $2\eta\dot{\gamma}$ (e.g. pressure solution creep), then an effective rheology is given by Eq. 1. This is a Bingham rheology (Fig. 1c-d), where viscous matrix creep occurs if bulk mélange stress $\tau_b \geq \phi\tau_y$. If the clast stress is too low for fracture, $\tau_b < \phi\tau_y$, it is assumed that the clasts deform by Newtonian creep with viscosity η_c (Eq. 1).

$$\begin{aligned} \tau_b &= \phi\tau_y + 2(1-\phi)\eta_m\dot{\gamma} \qquad \text{if } \tau \geq \phi\tau_y \\ \tau_b &= 2\left(\phi\eta_c + (1-\phi)\eta_m\right)\dot{\gamma} \quad \text{if } \tau < \phi\tau_y \end{aligned} \tag{1}$$

This simple model predicts that frictional failure and the activation of viscous flow occurs at a bulk stress which is lower than the frictional clast strength, as stress is focussed into only the clast volume (controlled by ϕ). This stress amplification has been shown to occur in models with complex force chain geometries, where frictional yield occurs for bulk stresses well below the clast yield limit due to the clast-matrix viscosity contrast (Beall et al., 2019). In the case of an idealized Bingham rheology with $\eta_c \to \infty$, Eq. 1 also predicts that the viscous strain-rate will be zero when frictional failure first occurs, as $\tau_{matrix} = 0$ when $\tau_b = \phi\tau_y$. A non-zero viscous strain-rate would then re-

quire τ_y to dynamically decrease or τ_b increase further. Clast stresses are not, however, likely to be homogeneous for realistic force chain geometries and matrix strain-rate will not be completely zero, so the predicted stress for the onset of visco-brittle deformation is an approximate guide.

3 Methodology

The modelling methodology is adapted from Beall et al. (2019), in which a Newtonian viscous mélange was modelled as elliptical clasts with 1:3 width:length ratios embedded in a matrix, where the clasts had a viscosity $10-10^4\times$ higher than the matrix and their sizes followed a power-law distribution. The velocity at the top boundary of the mélange was derived by applying a constant driving stress, allowing effective strain-rate, bulk viscosity and stress distribution to be calculated, as a function of viscosity contrast, clast proportion and shear zone thickness. Jamming of mélange with a viscosity contrast of 10^3 resulted in an effective viscosity increase of $2-7\times$ and clast shear stress of $6\tau_b-9\tau_b$ (for average driving stress τ_b applied at the shear zone boundary), over the range $0.5 \leq \phi \leq 0.64$. Here, we build upon these previous models by incorporating frictional failure into the clast rheology. This study also follows Webber et al. (2018), though is more simplified in order to characterise mélange rheology in a generalised manner.

Shear zone deformation is modelled as incompressible viscous flow, via the continuum-mechanics finite-element particle-in-cell code Underworld (Moresi et al., 2018), which solves the Stokes equations. The matrix has a Newtonian viscosity η_m, representing diffusion creep processes such as the pressure solution observed in quartz-phyllosilicate mixtures (Bos & Spiers, 2001; Fagereng & den Hartog, 2016; Niemeijer, 2018) at temperatures of $\geq 100^o$C and within a range of fine-grained metamorphic assemblages at lower crustal conditions (Wassmann & Stöckhert, 2013).

Clast regions also have a Newtonian viscosity set to $\eta_c = 10^3\eta_m$, representing a large viscosity contrast in the mélange. Where the maximum shear stress $\tau = (\sigma_1 - \sigma_2)/2$ (where σ_1 and σ_2 are the in-plane principal stresses) of a clast particle exceeds a frictional strength τ_y, an effective viscosity is calculated at that point in order to satisfy $\eta_f = \frac{1}{2}\tau_y/\dot{\gamma}$ (for maximum shear strain-rate $\dot{\gamma}$; following Fullsack, 1995; Moresi & Solomatov, 1998). This non-linearity is solved through successive Picard iterations for

each time-step, which terminate when the velocity field error has reduced by two orders of magnitude. The yield stress is set to the Mohr-Coulomb failure criteria (Eq. 2), for friction coefficient μ, cohesion C and effective mean stress σ_{eff} (Jaeger et al., 2007). We set $\mu = 0.7$ and $C = 50$ MPa, representing frictionally strong clasts (e.g. unfractured sandstone or basalt) close to Byerlee's law (Jaeger et al., 2007).

$$\tau_y = \frac{\mu\sigma_{eff} + C}{\sqrt{1+\mu^2}} \tag{2}$$

σ_{eff} is calculated as $(p + \rho g z)(1 - \lambda)$, where p is the average normal stress (the dynamic pressure) relative to the lithostatic pressure and is solved at each point every time-step, ρ is the average overburden density set to 2650 kg m^{-3}, g is gravitational acceleration, z is the overburden thickness and λ is the prescribed ratio of pore-pressure to lithostatic pressure. A small subset of test models (model-sets C and D) instead employs the Tresca criterion (constant τ_y), which can be attained by setting $\mu = 0$ in Eq. 2. We study deformation at a depth of z =40 km, roughly matching the depth of SSEs in Cascadia (Rogers & Dragert, 2003), southern Hikurangi (Wallace & Beavan, 2010) and the deep SSEs in Nankai (Obara et al., 2004). We assume $\lambda = 0.8$, which is intermediate between hydrostatic and lithostatic (Saffer & Tobin, 2011). This gives $\sigma_{eff} \approx$ 208 MPa (varying depending on p) for the models.

The model dimensions can be rescaled, in order to explore a wider parameter space. We assume that the model stress can be non-dimensionalised as in Eq. 3. The accuracy of this scaling should vary depending on the degree to which the bulk strain-rate of the mélange is a function of τ_y. It then follows that strain-rate $\dot{\gamma}$ can be non-dimensionalised as in Eq. 4. This scaling is tested by including the subset of models with a Tresca criterion (Table 2), which are run for both low and high τ_y (50 MPa and 200 MPa). The use of a constant τ_y within each model run of model-sets C and D simplifies this test, avoids the choice of whether μ or C is being varied and can be used to test the p dependence of the models with the Mohr-Coulomb criterion.

$$\tau_b' = \frac{\tau_b}{\tau_y} \tag{3}$$

$$\dot{\gamma}_b' = \dot{\gamma}_b \frac{\eta_m}{\tau_y} \tag{4}$$

Table 2. Summary of model-sets and parameters.

Model-set	Failure Criterion	Frictional Parameters	ϕ	D_{max}	Clast Size
A	Mohr-Coulomb	$\mu = 0.7$, $C = 50$MPa	0.3,0.5, 0.61	0.14, 0.28	power-law
B	Mohr-Coulomb	$\mu = 0.7$, $C = 50$MPa	0.3,0.5, 0.61	0.14, 0.28	uniform
C	Tresca	$\mu = 0$, $C = 200$MPa	0.61	0.14	power-law
D	Tresca	$\mu = 0$, $C = 50$MPa	0.61	0.14	power-law

A constant shear traction τ_b is applied to the top model wall, representing the bulk shear stress to drive deformation (e.g. Webber et al., 2018). A highly viscous Newtonian material with viscosity $10^3\eta_m$ is included in the upper 5% of the model domain, distributing this stress within the underlying mélange. The velocity magnitude is set to zero on the lower boundary. As the bulk rheology of the mélange is of primary interest, a bulk shear strain-rate $\dot{\gamma}$ is calculated as $0.5V_{av}/L$ for average horizontal velocity on the top wall V_{av} and model height L. The model width is $4L$ with periodic boundary conditions.

The ratio of the clast short-axis length to the shear zone width ($L = 100$m) is defined as D. For each ϕ, two sets of models are computed, one with D varying over $0.05 \leq D \leq 0.14$ (labelled as $D_{max} = 0.14$, Table 2) and another with $0.1 \leq D \leq 0.28$ ($D_{max} = 0.28$). $D_{max} = 0.14$ is likely to produce a force chain length scale which is smaller than L, while $D_{max} = 0.28$ is likely to produce force chains of length similar to L and the two choices of D_{max} are therefore less and more conducive to jamming, respectively (Beall et al., 2019). The element resolution is 2048×512 for models with $D_{max} = 0.14$, equivalent to a mesh node spacing of 4.9 cm for $L = 100$m. Models with $D_{max} = 0.28$ can be scaled to represent the same sized clasts in a thinner shear zone ($L = 50$ m) and therefore use a resolution of 1024×256 for consistent mesh node spacing.

While the models can be rescaled, we assume $L = 100$ m when $D = 0.14$ ($L = 50$ m when $D = 0.28$), reflecting typical active subduction shear-zone thicknesses (Rowe et al., 2013). This scale gives model clasts corresponding to blocks < 14 m long, which have been observed (Grigull et al., 2012). The clasts can also be considered as general strength heterogeneities.

All clasts have a short to long axis ratio of 3. The clast sizes of model-set A (Table 2) follow a power-law distribution with exponent -2, reflecting clast size distributions

in visco-brittle shear zones (Fagereng, 2011a; Grigull et al., 2012). As the clast size distributions are fractal (though limited to a minimum clast by the limited mesh resolution), the clast sizes can be scaled up to thicker shear zones with larger clasts or down to cm-m scale shear zones. Calculations of stress-strain-rate relationships are therefore approximately scale-invariant, provided our clast geometries and simplified rheologies hold. Such scaling is limited at the large scale by the largest clast dimension (blocks up to 100 m long have been observed; Grigull et al., 2012) and the breakdown of the simplified rheology at the small scale (grain-scale processes are critical at and below the mm scale; Fagereng & den Hartog, 2016). To test the effect of clast size distribution, model-set B is also included as an alternative end-member with uniform clast sizes of $D = D_{max}$.

Slip in SSEs ranges over the order of 1−100cm (Schwartz & Rokosky, 2007), which corresponds to relatively small strains of 10^{-5}−10^{-3} if distributed across 100 m thick shear zones as our models assume. In previous mélange models (Beall et al., 2019), force chains form from randomly distributed clasts after finite shear strains of about 1, and subsequently reorganise in response to shear strains of as little as 0.1. Because SSEs accommodate smaller strains than those involved in geometrical re-organisation within mélange, we assume that individual SSEs arise from temporal changes in rheology and have only minor geometrical effect. As the clasts are originally randomly orientated and with minimal force chains present, a 'warm-up model' is run for each ϕ up to a shear strain of $\gamma = 2$ to generate a strained mélange with force chains (if ϕ is sufficiently high). This is used as a starting geometry for the main model experiments. The setup runs neglect clast fracturing, for both computational efficiency and to provide equivalent starting conditions. The setup strain is sufficient for force chains to form (where ϕ is high enough), though further jamming may occur at higher strain. Mélange formation through disaggregation of stratigraphy and significant simple shear has been inferred to occur before and during lithification (Fagereng, 2011b; Festa et al., 2012). Our initial conditions could therefore apply to any depth. The models used in this analysis then begin at $\gamma = 2$ with the non-linear clast rheology incorporated and are run until $\gamma = 2.2$, at which point the mélange rheology is analyzed. While this strain is potentially large enough for force chain reorganisation, we do not observe significant temporal strength variations in any of the models.

Each numerical model is re-run for five different values of τ_b (21, 35, 70 and 140 MPa for the model-sets in Table 2), in order to calculate an effective relationship between

τ_b and $\dot{\gamma}_b$. 70 model-runs were therefore required to calculate effective rheologies for the 14 chosen parameter combinations (Table 2).

4 Results

4.1 Test of a Simplified Force Chain Model

We first test the applicability of Eq. 1, an idealized Voigt (iso-strain) mixture or Bingham rheology, to an idealized numerical model. The visco-brittle clast rheology is assigned to one column orientated at 45^o to the horizontal shear zone boundaries and parallel to the greatest compressive stress. This column represents a force chain, is assigned a constant $\tau_y = 170$ MPa, a width giving $\phi = 0.1$ and is embedded in a viscous matrix (Fig. 2a). Eq. 1 predicts onset of creeping for a bulk stress of 17 MPa. As the model is loaded parallel to the layering, its rheology should show excellent agreement with the Voigt mixture (Eq. 1). In the numerical model, the instantaneous strain-rate was calculated for a variety of boundary shear stress magnitudes. The simple force chain model exactly matches Eq. 1. The Bingham rheology therefore has the potential to capture the bulk rheology of a numerical model when the iso-strain (Voigt) assumption holds. Whether this holds for complicated force chain geometries is explored in the following sections.

4.2 Mélange Fracturing at Low Mélange Boundary Stress

We use model-sets A and B (Table 2) to test whether stress-amplification leads to significant fracturing even at bulk stresses much lower than the clast yield stress. For a depth of 40 km, fluid-pressure ratio $\lambda = 0.8$, the frictional parameters give a yield stress $\tau_y \approx 160$ MPa (varying slightly depending on p; Eq. 2). Results show that all models involved some clast yielding (ignoring yielding limited to clast edges) at the lowest applied stress $\tau_b = 21$ MPa (non-dimensionalised $\tau_b' = 0.13$), with the exception of the model with $\phi = 0.35$, $D = 0.14$ and uniform clast sizes, where clasts instead yielded at $\tau_b = 35$ MPa. Clast yielding results in a localized reduction in effective clast viscosity η_f by at least an order of magnitude (in order to satisfy $\tau = \tau_y$). Fracturing at $\tau_b = 21$ MPa is restricted to small isolated clasts ($D < D_{max}$) in models with power-law clast distributions and isolated clasts in models with uniform clast sizes.

As we are interested in how fracturing affects dynamics at the shear-zone scale, a lower threshold for broad-scale fracturing in models with $D = 0.14$ is quantified as the stress at which at least 4 of the largest clasts ($D = D_{max}$), about 25% of the large clasts when $\phi = 0.61$ (model-set A), have yielded. Broad-scale fracturing occurs at $\tau_b \geq 35$ MPa ($\tau_b' \geq 0.22$, Fig. 3) for models with $\phi = 0.61$, as well as $\phi = 0.5$ for uniform clast sizes. All other models have broad-scale fracturing when $\tau_b \geq 70$ MPa ($\tau_b' \geq 0.44$). These are conservative estimates as only 5 values of τ_b were sampled and are likely to be lower and differ for each ϕ. Significant fracturing can therefore occur when applied stress τ_b is substantially less than τ_y, particularly for jammed mélange and a volumetric clast proportion $> 50\%$, owing to stress amplification in the clasts.

Yielding by the Mohr-Coulomb failure criterion in the models is localized into conjugate sets of failure planes (Fig. 3). Conjugate sets should be symmetrical around σ_1 (which is 45^o clock-wise from the shear zone boundary for the dextral shear sense modelled), which is generally observed in the models (with minor deviation due to stress rotation). In contrast to a homogeneous incompressible material, the shear failure accommodates pure shear of the clasts, which are extended in the direction of σ_2, as evident in the final clast geometries (also observed in nature; Fagereng, 2013). Localized pure shear of the clasts occurs in the incompressible model because it is compensated by simple shear within the viscous matrix.

The Mohr-Coulomb failure criterion predicts that failure will predominately occur on planes orientated at angles $\pm tan^{-1}(\mu)/2 = \pm 17.5^o$ to σ_1. Numerical visco-plastic continuum-mechanical models only reproduce this Coulomb failure angle when a high resolution is used relative to initial stress perturbations and shear bands (Kaus, 2010), otherwise shear failure occurs on planes orientated closer to $\pm 45^o$ to σ_1 (called the Roscoe angles). Yielding zones localise in our models due to the pressure-dependence of the Mohr-Coulomb criteria, however are still relatively broad (< 10 m) as no strain softening was incorporated. Failure occurs along bands orientated at a range of angles between the Coulomb and Roscoe angles. The deviation from the Coulomb angles may be due to the mesh resolution being too coarse in places to sufficiently resolve stresses inside the clasts, though this deviation should not significantly affect clast deformation or stress magnitude.

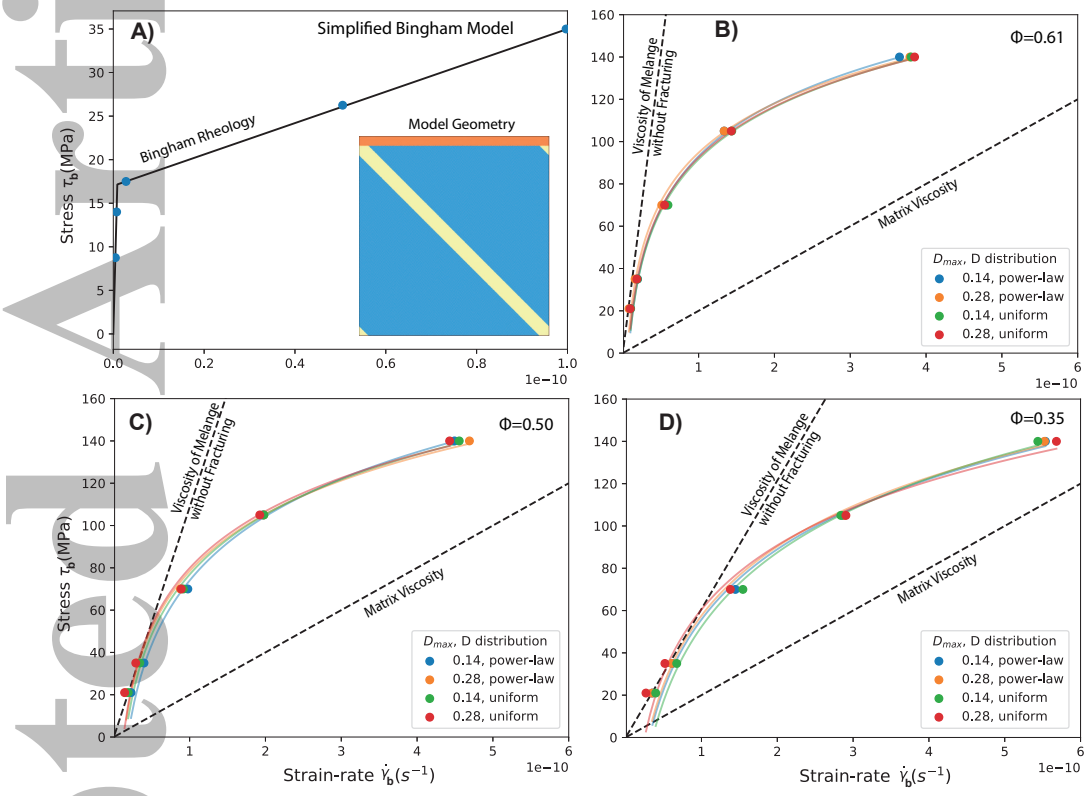

Figure 2. A) Idealized force chain model, consisting (inset) of clast material (yellow, $\phi = 0.1$) embedded in matrix (blue) with high viscosity material on top (orange). Measurements of τ_b (points) follow the Bingham plastic rheology (solid line, Eq. 1). B-D) Effective mélange rheologies of various parameter combinations in model-sets A and B (varied D_{max} and clast sizes either uniform or following a power-law distribution), grouped by ϕ and assuming $\eta_m = 10^{17}$ Pa s. Dashed lines show the Newtonian viscosities of the matrix material ($\phi = 0$) and of the mélange with fracturing disabled (for $\gamma = 2$, $D_{max} = 0.14$ and power-law clast distribution). Solid curves are logarithmic fits (Eq. 5).

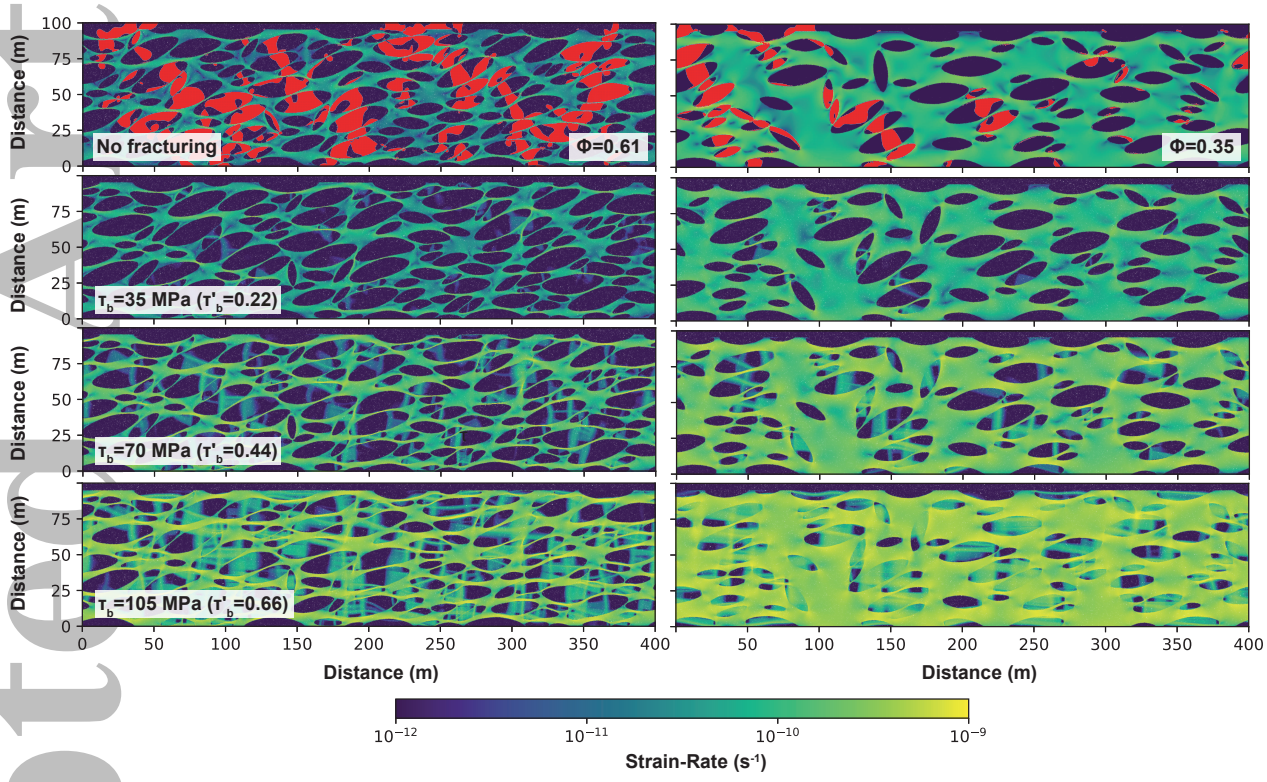

Figure 3. Mélange from model-set A with $\phi = 0.61$ (left) and $\phi = 0.35$ (right), $D_{max} = 0.14$ and $\eta_m = 10^{17}$ Pa s. For reference, the Newtonian 'warm-up models' ('no fracturing', the initial clast distribution for models with fracturing) are shown at $\gamma = 2$, for $\tau_b = 35$ MPa and regions with maximum shear stress increased above τ_b by $\geq 5\times$ colored red. Models with τ_b varying from 35 to 105 MPa are shown, demonstrating that the number of clasts reaching the frictional failure criterion increases dramatically with increasing τ_b and contributes to a significantly higher matrix strain-rate at high τ_b' compared to a linear rheology.

4.3 General Mélange Rheology

The effective mélange rheologies of each model-set and parameter combination are plotted in Fig. 2b-d. The models share some characteristics with the idealized Bingham rheology; at low applied stress the effective mélange viscosity can be much higher than η_m ($< 15\times$ for these models, depending on ϕ) and at high applied stress the behaviour is dominated by viscous matrix deformation (the slope $d\tau_b/d\dot{\gamma}_b$ is similar to that of the Bingham plastic prediction in Fig. 2a). However, for $\phi = 0.61$ and $\tau_b = 70$ MPa the fracturing causes the bulk strain-rate to be about $2\times$ higher than expected for the jammed mélange. This heralds a transition to predominately visco-brittle deformation, which occurs at a lower stress than the 100 MPa predicted for the simplified Bingham rheology. This is due to the heterogeneous stress distribution in the clasts, compared to the homogeneous stress assumed in the simplified model.

While the Bingham rheology is dominated by its viscous constituent when fracturing occurs, the corresponding mélange rheology appears to be best approximated by a logarithmic function (Eq. 5, for regression constants c_0 and c_1; curves in Fig. 2b-d). The fit is best for $\phi = 0.61$ and $\tau_b \geq 35$ MPa, the models with the most jamming and the τ_b at which rheology has diverged from the Newtonian mélange rheology. A power-law relationship of $\dot{\gamma} \propto \sigma^n$ does not provide a good fit (Fig. S2) and would give $n \sim 2$, rather than the $n > 10$ that would correspond to a highly non-linear rheology appropriate for a Reuss mixture. Eq. 5 is used as a simplified representation of the effective mélange rheology, which can be integrated into other models. It may be possible to derive a more accurate expression which captures the actual deformation mechanisms, however that is not our primary aim.

$$\tau_b = c_0 \ln(\dot{\gamma}_b) + c_1 \tag{5}$$

Mélange viscosity should always be greater than or equal to the matrix viscosity when $\tau_b \leq \tau_y$ and less or equal to an identical mélange in which fracturing is prohibited. These limits represent the stress end-members (dashed black lines, Fig. 2). All the model bulk rheologies, regardless of ϕ, follow a similar transition from one approximating the strong end-member (no fracturing) at the lowest τ_b (21 MPa or $\tau_b' = 0.13$), to resembling the weak end-member (matrix-dominated) for $\tau_b' \approx 0.75 - 0.9$ (the higher end of the range for greater ϕ). This rheological trend demonstrates that all mélange mod-

els, regardless of jamming, are weakened by fracturing even when $\tau_b < \tau_y$. While the bulk behaviour is bounded by the fracturing-free and clast-free viscosity end-members, fracturing of a jammed mélange results in higher strain-rate variation compared to these limiting cases (Fig. 2).

The exponential rheology $\tau_b \propto \ln(\dot{\gamma}_b)$ may arise because stress is not homogeneously distributed across force chains. The probability distribution of clast points with a particular maximum shear stress are shown in Fig. 4 for models with a range of τ_b. For $\tau_b =$ 21 and 35 MPa, the most common stress corresponds to the bulk shear stress τ_b. More clast particles have a stress higher than τ_b, than those with a stress lower than τ_b, resulting in a skewed normal distribution. Stresses higher than τ_b result from stress amplification within force chains, which occurs to a varying degree. Only a small number of force chains therefore fail when $\tau_b << \tau_y$. For an incremental increase in scaled stress τ_b' (corresponding to a τ_b increase or a τ_y decrease), a much higher number of clasts will fracture due to the non-linear stress distribution, which may explain the non-linear bulk rheology measured (in this case logarithmic). Stress cannot exceed the failure criterion, so with increasing τ_b, clast stress becomes more uniform as it is redistributed, resulting in a peak at τ_y in Fig. 4. By $\tau_b = 70MPa$ ($\tau_b' = 0.44$), most clasts are likely to be undergoing frictional failure.

The effective rheology depends primarily on ϕ, with only minor variation caused by changes in D_{max} and clast size distribution (Fig. 2b-d). The models with $\phi = 0.61$ have the most non-linear rheology, while the effective rheology is closest to the Newtonian matrix viscosity if $\phi = 0.35$. It was expected that larger D_{max} and uniform clast sizes would both promote jamming, however this was not consistently observed, probably indicating that their effect was of similar magnitude to that of the strain dependence (rheology was only measured at one γ) and the randomised clast placements. The highest mélange viscosity without fracturing was $24\eta_m$, for $D_{max} = 0.28$ and power-law clast distribution. This was much larger than the equivalent model with $D_{max} =$ 0.14, $14\eta_m$, although this appears to have a negligible effect on effective rheology. This is potentially because the asperity regions between clasts play a large role in Newtonian models but are easily disabled when a non-Newtonian clast rheology is considered.

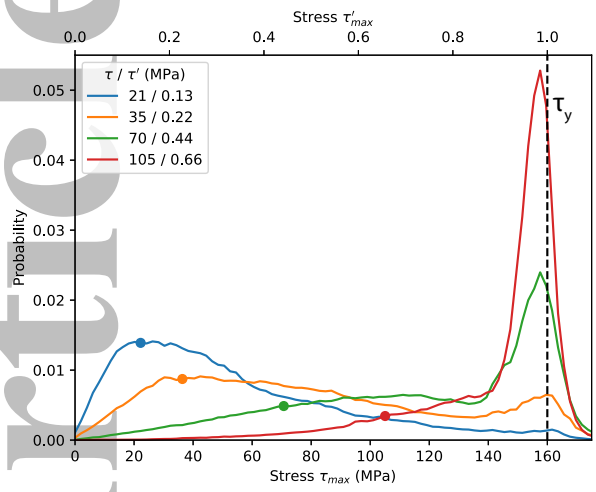

Figure 4. Maximum clast shear stress probability distribution, calculated from all Lagrangian particles identified as clast material, for $\phi = 0.61$, $D_{max} = 0.14$. $\mu = 0.7$ and $C = 50$ MPa ($\tau_y \approx 160$ MPa for $p \approx 0$; model-set A) and τ_b ranging from 21 to 105 MPa (bulk stresses shown by points). At low τ_b, stress follows a skew normal distribution, capturing heterogeneous stress amplification in force chains. At high τ_b, stress is limited by τ_y.

4.4 Frictional Weakening and Scaling

Two extra sets of models with $\phi = 0.61$ and a yield stress τ_y that is constant rather than dependent on dynamic pressure were run (B and C, Table 2), for $\tau_y = 50$ MPa and $\tau_y = 200MPa$, to explore how the visco-brittle mélange rheology depends on the magnitude of clast frictional strength. These models are used to test the hypothesised scaling relationships Eqns. 3 and 4, which can then be used to rescale the existing models for any τ_y and η_m.

When non-dimensionalised, all model-sets with $\phi = 0.61$ collapse onto the same curve as predicted by scaling relations (Fig. 5a). The non-dimensionalised datasets with $\mu = 0$ and $\mu = 0.7$ (pressure independent and dependent τ_y respectively) are identical, indicating that the pressure-dependence of the frictional law and therefore the optimal angle of frictional failure, does not influence the modelled bulk mélange viscosity. This is likely to be a result of the relatively high average normal stress in the absence of pressure perturbations, $(1 - \lambda)\,\rho g z = 208$MPa. Pressure-dependence of the failure criterion may play a larger role for smaller z or higher λ.

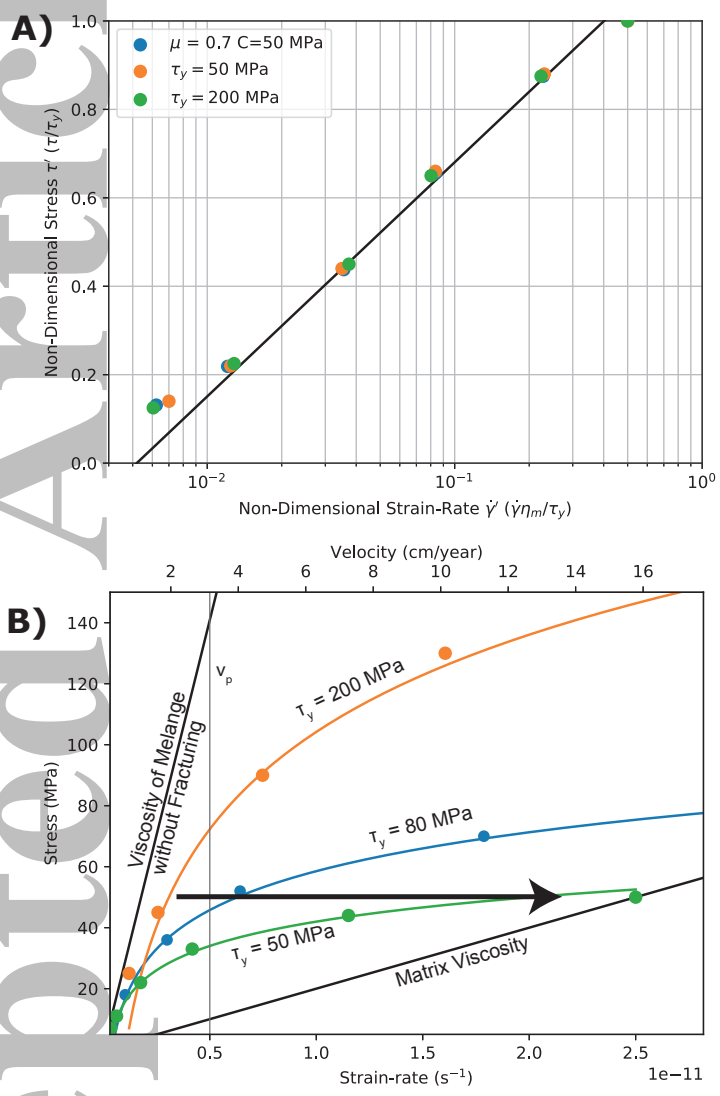

Figure 5. A) Model-sets A,C and D for $\phi = 0.61$ and $D_{max} = 0.14$, plotted for non-dimensional variables τ_b' and $\dot{\gamma}_b'$ (Eqs. 3 and 4). All data collapses onto one curve, confirming the scaling of stress using τ_y. Eq. 5 is plotted (non-dimensionalised) for $c_0 = 0.23$ and $c_1 = 1.21$. B) Model sets B and C, with a third case for $\tau_y = 80$ MPa plotting using the scaling relationship and assuming $\eta_m = 10^{18}$ Pa s. The logarithmic fit from A is plotted for each dataset. Velocity is calculated assuming $L = 100$ m. A plate velocity of $V_p = 10^{-9}$ m s^{-1} is shown. In the case of a constant $\tau_b = 50$ MPa, deformation of mélange containing clasts with a high frictional strength, $\tau_y = 200$ MPa, results in a velocity of 2 cm yr^{-1}. Reducing the clast frictional strength to 50 - 80 MPa (indicated by arrow) would increase this to 4 - 16 cm yr^{-1}.

The scaling relationships can be used to approximately estimate the driving stress required to initiate tensile failure in multiple clasts, which occurs in jammed mélange for at least $\tau_b' = 0.22$. Tensile failure occurs when $\tau_y = \sigma_{eff} + T$, for tensile strength T. Estimates of C/T vary over 2 to ≈15 (Sibson, 1998; Jaeger et al., 2007). As $\sigma_{eff} \approx$ 208 MPa (varying from this value for non-zero p), $3.5 \leq T \leq 25$. For $z = 40$ km and $\lambda = 0.8$, tensile fracture is predicted by 211 MPa $\leq \tau_y \leq$ 233 MPa. Tensile fracture could therefore occur when 46 MPa $\leq \tau_b \leq$ 51 MPa ($\tau_b' = 0.22$), which is plausible for subduction shear zones. Tensile fractures are commonly observed in subduction mélange and their preferential failure, rather than shear, is likely to require factors not modelled here, such as higher λ, the inheritance of preferential failure planes (failure criteria assume failure planes exist in all orientations), or dynamic pressure variations influenced by matrix anisotropy (e.g Fagereng et al., 2010).

Fig. 5b demonstrates how strain-rate, and therefore velocity at the shear zone wall, would increase if τ_y were decreased for all clasts from 200 MPa to 50 MPa. The scaling relationships are also used to calculate an intermediary case of $\tau_y = 80$ MPa. For $\eta_m = 10^{18}$ Pa s (assumed for Fig. 5b) and $L = 100$m, the average shear zone boundary velocity V_{av} is about 2 cm/yr when $\tau_b = 50$ MPa and $\tau_y = 200$ MPa. This is equivalent to $\tau_b' = 0.25$, which is sufficient for fracturing of clasts in the force chains with the highest stress amplification (similar to Fig. 3b). In order to increase the velocity to 4 cm/yr, the clast yield strength needs to be reduced to $\tau_y = 80$ MPa. Should τ_y decrease to $\tau_y = 50$ MPa, the velocity would increase by 8× up to 16 cm/yr and the matrix would have a similar stress state to the clasts. This example demonstrates that τ_b' must be initially relatively low and τ_y must decrease dramatically, in order to generate a large strain-rate transient.

4.5 Spring-Block Slider Models

The conceptual model of cyclic strain-rate transients driven by variation of clast friction (Fig. 5b) is now demonstrated with simplified spring-block slider models with only one degree of freedom. Such models are used to quantify the most simplified dynamic interplay between fault slip with variable friction and elastic loading (Gu et al., 1984; Rice & Tse, 1986), and are useful for exploring the fundamental behaviour of a system (such as stability) before moving to more complex models. The block displacement x of a spring-block slider neglecting inertia and seismic radiation (we assume viscous damp-

ing dominates), is calculated by solving Eq. 6 for V and integrating over discrete time-steps (methods further described in S2 and S3). The plate velocity V_p (set to 10^{-9} m s^{-1} or ≈ 3 cm yr^{-1}) loads the spring, while shear deformation unloads it. The spring stiffness k is set to 10^8 Pa m^{-1}, chosen for consistency with the second slider example. The bulk rheology may depend on τ_b, γ_b or a state variable θ, depending on the choice of τ_b.

$$k(V_p t - x) = \tau_b(\tau, V, \theta) \tag{6}$$

The mélange weakening example illustrated in Fig. 5b is demonstrated by setting τ_b to the logarithmic function (Eq. 5) fitted to the model with $\phi = 0.61$, $D = 0.14$ and clast sizes following a power-law distribution (Figs. 5 and S2). The most simplified spring-block slider model approach is taken, incorporating friction which discretely steps between static and dynamic values. The yield stress, τ_y, is reduced to τ_{y1} when the shear stress acting on the slider (τ_b) reaches a critical stress (τ_1). As the resulting shear deformation lowers the shear stress on the block from τ_1 to τ_0, the yield stress recovers to a value τ_{y0}.

$$\begin{aligned} \tau_y &= \tau_{y1} \quad \text{if } \tau_b \geq \tau_1 \\ \tau_y &= \tau_{y0} \quad \text{if } \tau_b \leq \tau_0 \end{aligned} \tag{7}$$

We assume that that $\tau_{y0} = 200$ MPa. The rheology with $\tau_y = 200$ MPa in Fig. 5b will deform at the same rate as V_p ($\dot{\gamma} = 5 \times 10^{-12}$) for $\tau_b = 72$ MPa, while elastic strain will accumulate at lower stress. Following the example in Fig. 5b, it is assumed that the slider stress is $\approx$ 50 MPa ($\tau_b' = 0.25$). We assume that clast weakening occurs when τ_b reaches $\tau_1 = 50$ MPa, which is plausible given that pervasive force chain fracturing occurs at least when $\tau_b' \approx 0.2$ in the mélange models. Assuming for simplicity a stress drop of 1 MPa gives $\tau_0 = 49$ MPa. Mélange models with varied τ_{y0} are shown in Fig. 6a and show that τ_y must be reduced by 75% to increase V to $4V_p$ ($\approx 5V_p$ taking into account the deviation of Eq. 1 at $\tau' \approx 1$). The bulk mélange rheology therefore requires a large $\Delta\tau_y = \tau_{y1} - \tau_{y0}$ to produce strain-rate transients analogous to SSEs, while τ_1 must be low enough for elastic strain to accumulate.

While clast friction was assumed to vary instantaneously, the rate of friction variation competes with elastic unloading and viscous deformation, which may prevent strain-

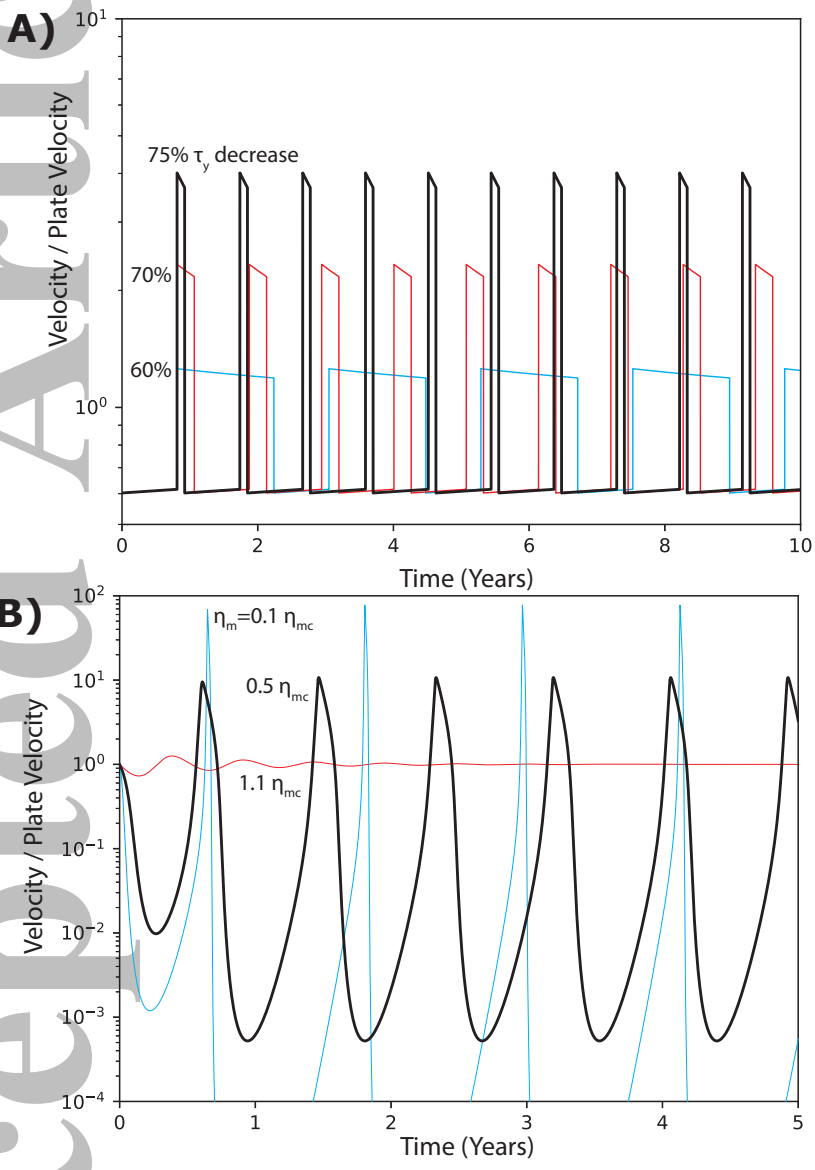

Figure 6. Spring-block slider models employing the logarithmic rheology fitted from the numerical model in Fig. 5b and instantaneous frictional weakening (A) and employing the simplified Bingham rheology with rate-and-state friction (B). A) Models with varying τ_{y1} as a percentage decrease from $\tau_{y0} = 200$ MPa. B) Models with varying η_m as a percentage of the critical matrix viscosity.

rate transients. We model this interaction by incorporating rate-and-state friction into the spring-block slider, which models the dependence of τ_y on V and θ according to Eq. 8 (Scholz, 1998). State is assumed to vary according to the aging law (Eq. 9). μ_0 is steady-state friction, a and b are parameters which control velocity strengthening ($a-b>0$) or weakening ($a-b<0$), V_0 is a reference velocity and D_c is the characteristic slip distance. As there are many variables and rate-and-state behaviour is complex, Eq. 8 is incorporated into the simplified Bingham rheology (Eq. 1; neglecting clast viscosity), such that the parameters of the system close to stability can be predicted. We assume values of $a = 10^{-3}$, $b = 6 \times 10^{-3}$ (rate-weakening), $\mu_0 = 0.6$, $D_c = 10^{-3}$ m and $V_0 = 10^{-6}$m/s, representing typical experimental data and D_c scaled up for a fault-zone (Marone, 1998). σ_{eff} is kept at 200 MPa and η_m is varied. ϕ is initially set to 0.6. The chosen $k = 10^8$ Pa/m is equivalent to 10% of the critical stiffness for instability of a regular rate-and-state slider with these parameters (Eq. S3). The variation of these parameters affect the stress drop, peak velocity and recurrence time of slip events, however we focus on the existence of periodic slip events and their dependence on η_m.

$$\tau_y = \sigma_{eff}\left(\mu_0 + a\ln\left(\frac{V}{V_0}\right) + b\ln\left(\frac{V_0\theta}{D_c}\right)\right) \tag{8}$$

$$\frac{d\theta}{dt} = 1 - \frac{V\theta}{D_c} \tag{9}$$

Episodic strain-rate transients can be produced by a Bingham rheology incorporating rate-and-state friction (Fig. 6b). A critical matrix viscosity η_{mc} can be calculated (Eq. 10, derived in S3), analogous to the critical stiffness, above which viscous damping forces a decay to a steady velocity and below which an oscillation is possible. For our chosen parameters, $\eta_{mc} = 1.25 \times 10^{17}$ Pa s.

$$\eta_{mc} < \frac{(\phi(b-a)\sigma_{eff} - kD_c)\,L}{(1-\phi)V_p} \tag{10}$$

Matrix viscosity of $0.5\eta_{mc}$ produces peak velocities of $10V_p$, while the velocity of a slider with $1.1\eta_{mc}$ quickly decays to V_p. The Bingham spring-block slider therefore resembles a regular spring-block slider with rate-and-state friction, however its peak velocity and minimum ϕ are limited by viscous damping (Fig. S3). A viscosity $0.1\eta_{mc}$ results in peak velocities of $100V_c$, which is approximately the upper bound of observed

SSE velocities. Models with $0.5\eta_{mc}$ and $0.1\eta_{mc}$ have stress drops of 2 and 3.5 MPa respectively, lower than the $\Delta\tau_y$ of 5.5 MPa and 8 MPa (Fig. S4) as a result of the stress partitioning controlled by ϕ. A small ϕ results in focussing of τ_b into a smaller clast volume and therefore increased stress amplification. It is unclear how ϕ should be related between the idealized Bingham and mélange models, as strength amplification in the latter is much greater. A lower $\phi = 0.2$ reduces the stress drops to 0.6 and 1 MPa, with $\Delta\tau_y = 3.5$ and 6.5 MPa, for the same peak velocities, however η_{mc} is reduced to 1.25×10^{16} Pa s (Fig. S5). These examples demonstrate that a Bingham rheology with clasts following rate-and-state friction and realistic parameters are capable of producing slip transients at η_m on the order of $10^{16} - 10^{17}$ Pa s and stress drops of a few MPa.

5 Discussion

We previously predicted, and have tested here, that fracturing could occur at relatively low applied shear stress in a mélange due to stress amplification, increasing $\dot{\gamma}_b$ (Beall et al., 2019, Fig. 1a-b). Fracturing of clasts involved in force chains does occur at low bulk stress, lowering the stress within the most load-bearing force chains. The fracturing also allows matrix strain-rate to increase. We found that clast fracturing can occur when $\tau_b \approx 35$ MPa and $\lambda = 0.8$, even at 40 km depth. More generally, fracturing of multiple force chain clasts within a jammed mélange ($\phi = 0.61$; Figs. 3 and 4) occurs $\tau_b \geq 0.22\tau_y$, which is a conservative estimate due to the sparse sampling of τ_b. Fracturing of clasts within a mélange therefore may be as indicative of a large strength contrast between the matrix and clast, as of extreme pore pressure (e.g. Webber et al., 2018).

The models verify that deformation of jammed mélange switches from clast to matrix dominated with increasing bulk stress, analogous to the Bingham model. In a mixture of strong frictional clasts and weak viscous matrix, mixed visco-brittle deformation may record periods of high stress and/or weakened clasts and therefore high strain-rates (creating slip transients, e.g. SSEs), the duration of which may be related to transient local variations in effective stress and healing of fractures. Fracturing at low τ_b does not, however, result in the dramatic switch to viscous deformation predicted by the Bingham model. This is because clast stresses follow a skew normal distribution and weakening of a force chain with the highest stress amplification does not weaken the force chains with less stress amplification (Fig. 4). Clast yielding also reduces the effective strength

contrast between mélanges of varying thickness previously calculated for Newtonian rheologies (Beall et al., 2019), which depends on asperities which fail at low τ_b.

The rheology of a jammed mélange appears to be best approximated by a logarithmic function of $\dot{\gamma}$, likely related to the varying distribution of fractured clasts at different τ_b as each increment of stress weakens a greater number of force chains at higher stress. Strain-rate variation therefore results from changes to the proportion of clasts undergoing frictional failure. Weakening of one force chain will lead to stress redistribution and an entire shear zone may be unjammed if clast weakening is high.

Compared to the weak stress-dependence of frictional sliding, viscous systems are extremely damped (stress-dependent). The visco-brittle composites modelled here require variations in loading or internal frictional strength of order ranging $1-100$ MPa to produce slip transients comparable to SSEs, significantly higher than the $10 - 100$ kPa order variation in τ_b calculated for SSE models using typical rate-and-state friction (e.g. Rubin, 2008). The Bingham model with rate-and-state friction represents idealized jamming, so the estimates of 3.5 MPa $\leq \Delta\tau_y \leq$ 8 MPa to produce $10V_p \leq V \leq 100V_p$ are lower bounds (depending on η_m relative to the critical viscosity, and ϕ). The mélange models are less jammed than the Bingham model, resulting in a more gradual increase in $\dot{\gamma}_b$ with τ_b (Fig. 2). The mélange models subsequently require a much higher 120 MPa $\leq \Delta\tau_y \leq$ 150 MPa for $1.2V_p \leq V \leq 5V_p$.

Real mélange is likely to be some combination of the logarithmic mélange and idealized Bingham rheologies, when the anisotropy and possible non-linearity of the matrix rheology is considered. Ando et al. (2012) assumed that $\Delta\tau_y$ is equivalent to SSE stress drop (typically only 10-100 kPa; Brodsky & Mori, 2007) and as a result predicted an extremely low $\eta_m \sim 10^{11}$ Pa s in order to reproduce SSE velocities. In both the mélange and idealized Bingham models, a large $\Delta\tau_y$ may not be reflected in τ_b variation, as τ_b is buffered by stress redistribution into matrix deformation. SSE generation due to visco-brittle interaction is therefore likely to require severe frictional weakening, which may not manifest in inferred stress drop.

The spring-block slider models demonstrate that weakening of brittle clasts in a visco-brittle mixture could in principle generate strain-rate transients equivalent to SSEs, which are likely to be controlled by η_m, the frictional properties of the clasts and the degree of jamming. η_m is required to be low enough that it can accommodate the high strain-

rate during a SSE, characterised by the critical viscosity when rate-and-state friction was considered, which in our models was of the orders $10^{16}-10^{18}$Pa s. This is relatively low, but could be reconciled with pressure-solution creep (Niemeijer, 2018) or phyllosilicate flow laws (Mares & Kronenberg, 1993; Hilairet et al., 2007). It is also encouraging that a Bingham rheology integrating rate-and-state friction, with parameters mostly typical of experimental values, can sustain episodic slip. However, the system explored is highly simplified and a higher dimension model with an elastic half-space is necessary for predicting recurrence times, stress drops and peak velocities relevant to actual subduction zones. The prediction of η_{mc} can be used to guide the parameter exploration of these future models.

The degree of frictional weakening predicted is significantly higher than the $\sim 1\%$ weakening typical of frictional sliding at $\sim 10^{-4}$ m s^{-1} (Marone et al., 1990), however the Bingham slider model predicts that the frictional weakening typical of higher velocities could occur at lower velocities limited by viscous deformation. Frictional weakening in the rate-and-state model has been related to dilation, which could manifest at the outcrop scale as the opening of extension or extensional-shear fractures in clasts. Such through-going fractures with a tensile component are commonly observed in mélange clasts, and can be confined to the clasts and form at an angle of 80^o to discrete shear surfaces parallel to the shear zone S-fabric (Fisher & Byrne, 1987; Fagereng, 2011b, 2013). These fractures accommodate extension of the clasts (pure shear), which is kinematically consistent with simple shear partitioned into and accommodated by the matrix. The mélange models also deform by this combination of clast pure shear and matrix simple shear.

Simple shear of mélange may occur by combined deformation of a network of visco-brittle matrix shears and connecting tensile fractures as described in several field examples (Sibson, 1996; Meneghini & Moore, 2007; Fagereng et al., 2010; Ujiie et al., 2018). Such shear-fracture meshes within a ductile matrix are analogous to our model, which is rate-limited by viscous deformation when clast fracturing occurs. This model of local fracturing limited by surrounding ductile creep applies when there is no interconnected network of frictional material in the direction of simple shear. In our models, this condition is guaranteed by the assumption of a viscous matrix, however, extrapolation to nature requires that any fractures within the matrix (not modelled here) do not extend/connect to form a more extensive shear fracture network. If localized shears do develop in the matrix, experiments indicate that these may favour development of frictional instabil-

ities, but slip speed is still modulated by their interaction with surrounding creeping matrix (Scuderi et al., 2017).

6 Conclusion

We have characterised the bulk rheology of a mélange consisting of strong visco-brittle clasts embedded in a weak viscous matrix using numerical visco-plastic finite element models. When the clasts form a stress-bearing force-chain network, the bulk viscosity of the mélange can be more than an order of magnitude stronger than the matrix viscosity, in the absence of clast fracturing. When fracturing is allowed, clasts within the most load-bearing force chains undergo frictional failure in models with bulk stress far below the clast frictional strength, $\tau_b \geq 0.22\tau_y$, because of the stress amplification that occurs within a shear zone with high viscosity contrasts. The fracturing of clasts acts to homogenize stress in the force chain network and redistribute stress into viscous matrix deformation. As deformation is limited by clast friction at low stress and rate-strengthening viscous matrix creep at high stress, mélange rheology resembles a Bingham plastic. However, unlike a Bingham plastic, the switch from brittle to viscous deformation occurs gradually, due to the heterogeneity of force chain stresses. This transition results in an effective rheology in the form of $\dot{\gamma}_b \propto \ln(\tau_b)$, as the number of clasts fracturing is more stress-sensitive at higher stress. This gradual transition also requires a large stress increase or clast yield strength decrease ($> 70\%$) in order to produce significant bulk strain-rate increase ($\sim 8\times$).

The models demonstrate how damped (i.e. significantly rate-strengthening) a visco-brittle shear zone can be when no frictional slip surface spans it. Such a damped system could still generate a period of high strain-rate, as demonstrated by simple spring-block slider models. Matrix viscosities ranging over the orders 10^{16}-10^{18} Pa s (depending on the visco-brittle formulation) could be reconciled with SSEs, comparable to rheological estimates. We suggest that this frictional weakening could occur due to the opening of extension or extensional-shear fractures. This prediction needs to be tested through future modelling incorporating tensile fracturing and elasticity. Simple shear across the modelled shear zone is accommodated by extension of clasts (pure shear) and simple shear of the matrix. This model is supported by observed shear networks in exhumed mélange. The incorporation of viscous damping into SSE rupture models is likely to permit aseis-

mic SSEs for a wider range of conditions than presently thought, explaining their ubiquity in subduction zones globally.

Acknowledgments

This project has received funding from the European Research Council (ERC) under the European Union's Horizon 2020 research and innovation program (starting grant agreement 715836 MICA). The Hawk computing cluster (Cardiff University) was used for all numerical calculations. We acknowledge the support of the Supercomputing Wales project, which is part-funded by the European Regional Development Fund (ERDF) via Welsh Government. Ellis was supported by MBIE Endeavour and core research funds to GNS Science. The open-source geodynamic code Underworld is available at http://www.underworldcode.org, and model parameters required to replicate the results are detailed in the manuscript. The spring-block slider models are available at https://doi.org/10.5281/zenodo.3403261. Constructive reviews from two anonymous reviewers and the editorial guidance of T.W. Becker greatly improved the manuscript.

References

Ando, R., Takeda, N., & Yamashita, T. (2012). Propagation dynamics of seismic and aseismic slip governed by fault heterogeneity and Newtonian rheology. *Journal of Geophysical Research B: Solid Earth*, *117*(11), 1–14. doi: 10.1029/2012JB009532

Beall, A., Fagereng, Å., & Ellis, S. (2019). Strength of Strained Two-Phase Mixtures: Application to Rapid Creep and Stress Amplification in Subduction Zone Mélange. *Geophysical Research Letters*. doi: 10.1029/2018GL081252

Behr, W. M., & Becker, T. W. (2018). Sediment control on subduction plate speeds. *Earth and Planetary Science Letters*. doi: 10.1016/j.epsl.2018.08.057

Birren, T., & Reber, J. E. (2019). The impact of rheology on the transition from stick-slip to creep in a semi-brittle analog. *Journal of Geophysical Research: Solid Earth*. doi: 10.1029/2018jb016914

Bos, B., & Spiers, C. J. (2001). Experimental investigation into the microstructural and mechanical evolution of phyllosilicate-bearing fault rock under conditions favouring pressure solution. *Journal of Structural Geology*. doi: 10.1016/S0191-8141(00)00184-X

Brodsky, E. E., & Mori, J. (2007). Creep events slip less than ordinary earthquakes. *Geophysical Research Letters*. doi: 10.1029/2007GL030917

Dragert, H., Wang, K., & James, T. S. (2001). A silent slip event on the deeper Cascadia subduction interface. *Science*. doi: 10.1126/science.1060152

Duarte, J. C., Schellart, W. P., & Cruden, A. R. (2015). How weak is the subduction zone interface? *Geophysical Research Letters*. doi: 10.1002/2014GL062876

Fagereng, Å. (2011a). Frequency-size distribution of competent lenses in a block-in-matrix mélange: Imposed length scales of brittle deformation? *Journal of Geophysical Research: Solid Earth*. doi: 10.1029/2010JB007775

Fagereng, Å. (2011b). Geology of the seismogenic subduction thrust interface. *Geological Society, London, Special Publications*, *359*(1), 55–76. doi: 10.1144/SP359.4

Fagereng, Å. (2013). On stress and strain in a continuous-discontinuous shear zone undergoing simple shear and volume loss. *Journal of Structural Geology*, *50*, 44–53. doi: 10.1016/j.jsg.2012.02.016

Fagereng, Å., & den Hartog, S. A. M. (2016). Subduction megathrust creep governed by pressure solution and frictionalviscous flow. *Nature Geoscience*. doi: 10.1038/ngeo2857

Fagereng, Å., Hillary, G. W. B., & Diener, J. F. A. (2014). Brittle-viscous deformation, slow slip, and tremor. *Geophysical Research Letters*. doi: 10.1002/2014GL060433

Fagereng, Å., Remitti, F., & Sibson, R. H. (2010). Shear veins observed within anisotropic fabric at high angles to the maximum compressive stress. *Nature Geoscience*. doi: 10.1038/ngeo898

Fagereng, Å., & Sibson, R. H. (2010). Mélange rheology and seismic style. *Geology*, *38*(8), 751–754. doi: 10.1130/G30868.1

Festa, A., Dilek, Y., Pini, G. A., Codegone, G., & Ogata, K. (2012). Mechanisms and processes of stratal disruption and mixing in the development of mélanges and broken formations: Redefining and classifying mélanges. *Tectonophysics*. doi: 10.1016/j.tecto.2012.05.021

Fisher, D., & Byrne, T. (1987). Structural evolution of underthrusted sediments, Kodiak Islands, Alaska. *Tectonics*. doi: 10.1029/TC006i006p00775

Fullsack, P. (1995). An arbitrary LagrangianEulerian formulation for creeping flows and its application in tectonic models. *Geophysical Journal International*. doi: 10.1111/j.1365-246X.1995.tb05908.x

Goswami, A., & Barbot, S. (2018). Slow-slip events in semi-brittle serpentinite fault zones. *Scientific Reports*. doi: 10.1038/s41598-018-24637-z

Grigull, S., Krohe, A., Moos, C., Wassmann, S., & Stöckhert, B. (2012). "Order from chaos": A field-based estimate on bulk rheology of tectonic mélanges formed in subduction zones. *Tectonophysics*, *568-569*, 86–101. doi: 10.1016/j.tecto.2011.11.004

Gu, J.-C., Rice, J. R., Ruina, A. L., & Tse, S. T. (1984). Slip motion and stability of a single degree of freedom elastic system with rate and state dependent friction. *Journal of the Mechanics and Physics of Solids*, *32*(3), 167–196. doi: 10.1016/0022-5096(84)90007-3

Handy, M. R. (1994). Flow laws for rocks containing two non-linear viscous phases: A phenomenological approach. *Journal of Structural Geology*. doi: 10.1016/0191-8141(94)90035-3

Hayman, N. W., Ducloué, L., Foco, K. L., & Daniels, K. E. (2011). Granular Controls on Periodicity of Stick-Slip Events: Kinematics and Force-Chains in an Experimental Fault. *Pure and Applied Geophysics*. doi: 10.1007/s00024-011-0269-3

Hayman, N. W., & Lavier, L. L. (2014). The geologic record of deep episodic tremor and slip. *Geology*, *42*(3), 195–198. doi: 10.1130/G34990.1

Hilairet, N., Reynard, B., Wang, Y., Daniel, I., Merkel, S., Nishiyama, N., & Petitgirard, S. (2007). High-pressure creep of serpentine, interseismic deformation, and initiation of subduction. *Science*. doi: 10.1126/science.1148494

Hyndman, R. D., Yamano, M., & Oleskevich, D. A. (1997). The seismogenic zone of subduction thrust faults. *Island Arc*. doi: 10.1111/j.1440-1738.1997.tb00175.x

Jaeger, J. C. J. C., Cook, N. G. W., & Zimmerman, R. W. (2007). *Fundamentals of rock mechanics*. Blackwell Pub.

Kaproth, B. M., & Marone, C. (2013). Slow earthquakes, preseismic velocity changes, and the origin of slow frictional stick-slip. *Science*. doi: 10.1126/science.1239577

Karato, S.-i. (2012). *Deformation of Earth Materials*. doi: 10.1017/

cbo9780511804892

Kaus, B. J. P. (2010). Factors that control the angle of shear bands in geodynamic numerical models of brittle deformation. *Tectonophysics*. doi: 10.1016/j.tecto .2009.08.042

Kitamura, Y., Sato, K., Ikesawa, E., Ikehara-Ohmori, K., Kimura, G., Kondo, H., ... Masago, H. (2005). Mélange and its seismogenic roof décollement: A plate boundary fault rock in the subduction zone - An example from the Shimanto Belt, Japan. *Tectonics*. doi: 10.1029/2004TC001635

Lavier, L. L., Bennett, R. A., & Duddu, R. (2013). Creep events at the brittle ductile transition. *Geochemistry, Geophysics, Geosystems*. doi: 10.1002/ggge .20178

Leeman, J. R., Marone, C., & Saffer, D. M. (2018). Frictional Mechanics of Slow Earthquakes. *Journal of Geophysical Research: Solid Earth*. doi: 10.1029/ 2018JB015768

Li, S., Freymueller, J., & McCaffrey, R. (2016). Slow slip events and time-dependent variations in locking beneath Lower Cook Inlet of the Alaska-Aleutian subduction zone. *Journal of Geophysical Research: Solid Earth*. doi: 10.1002/2015JB012491

Liu, Y., & Rice, J. R. (2005). Aseismic slip transients emerge spontaneously in three-dimensional rate and state modeling of subduction earthquake sequences. *Journal of Geophysical Research: Solid Earth*. doi: 10.1029/2004JB003424

Luo, Y., & Ampuero, J. P. (2018). Stability of faults with heterogeneous friction properties and effective normal stress. *Tectonophysics*. doi: 10.1016/j.tecto .2017.11.006

Mares, V. M., & Kronenberg, A. K. (1993). Experimental deformation of muscovite. *Journal of Structural Geology*. doi: 10.1016/0191-8141(93)90156-5

Marone, C. (1998). Laboratory-derived friction laws and their application to seismic faulting. *Annual Review of Earth and Planetary Sciences*, *26*(1), 643–696. doi: 10.1146/annurev.earth.26.1.643

Marone, C., Raleigh, C. B., & Scholz, C. H. (1990). Frictional behavior and constitutive modeling of simulated fault gouge. *Journal of Geophysical Research*. doi: 10.1029/JB095iB05p07007

Meneghini, F., & Moore, J. C. (2007). Deformation and hydrofracture in a sub-

duction thrust at seismogenic depths: The Rodeo Cove thrust zone, Marin Headlands, California. *Bulletin of the Geological Society of America*. doi: 10.1130/B25807.1

Moresi, L., Mansour, J., Giordani, J., Farrington, R., & Beucher, R. (2018). *Underworld 2.* Retrieved from `https://doi.org/10.5281/zenodo.1434224` doi: 10.5281/zenodo.1434224

Moresi, L., & Solomatov, V. (1998). Mantle convection with a brittle lithosphere: throughts on the global tectonic styles of the Earth and Venus. *Geophysical Journal International*. doi: 10.1046/j.1365-246X.1998.00521.x

Niemeijer, A. R. (2018, dec). Velocity-dependent slip weakening by the combined operation of pressure solution and foliation development. *Scientific Reports*, *8*(1), 4724. doi: 10.1038/s41598-018-22889-3

Obara, K., Hirose, H., Yamamizu, F., & Kasahara, K. (2004). Episodic slow slip events accompanied by non-volcanic tremors in southwest Japan subduction zone. *Geophysical Research Letters*. doi: 10.1029/2004GL020848

Reber, J. E., Lavier, L. L., & Hayman, N. W. (2015). Experimental demonstration of a semi-brittle origin for crustal strain transients. *Nature Geoscience*. doi: 10.1038/ngeo2496

Rice, J. R., & Tse, S. T. (1986). Dynamic motion of a single degree of freedom system following a rate and state dependent friction law. *Journal of Geophysical Research*, *91*(B1), 521–530. doi: 10.1029/JB091iB01p00521

Rogers, G., & Dragert, H. (2003). Episodic tremor and slip on the Cascadia subduction zone: The chatter of silent slip. *Science*, *300*(5627), 1942–1943. doi: 10.1126/science.1084783

Rowe, C. D., Meneghini, F., & Moore, J. C. (2011). Textural record of the seismic cycle: strain-rate variation in an ancient subduction thrust. *Geological Society, London, Special Publications*. doi: 10.1144/SP359.5

Rowe, C. D., Moore, J. C., & Remitti, F. (2013). The thickness of subduction plate boundary faults from the seafloor into the seismogenic zone. *Geology*. doi: 10.1130/G34556.1

Rubin, A. M. (2008). Episodic slow slip events and rate-and-state friction. *Journal of Geophysical Research: Solid Earth*. doi: 10.1029/2008JB005642

Saffer, D. M., & Tobin, H. J. (2011). Hydrogeology and Mechanics of Subduction

Zone Forearcs: Fluid Flow and Pore Pressure. *Annual Review of Earth and Planetary Sciences*. doi: 10.1146/annurev-earth-040610-133408

Schmid, D. W., & Podladchikov, Y. Y. (2003). Analytical solutions for deformable elliptical inclusions in general shear. *Geophysical Journal International*, *155*(1), 269–288. doi: 10.1046/j.1365-246X.2003.02042.x

Scholz, C. H. (1998). Earthquakes and friction laws. *Nature*, *391*(6662), 37–42. doi: 10.1038/34097

Schwartz, S. Y., & Rokosky, J. M. (2007, sep). *Slow slip events and seismic tremor at circum-pacific subduction zones* (Vol. 45) (No. 3). Wiley-Blackwell. doi: 10.1029/2006RG000208

Scuderi, M. M., Collettini, C., Viti, C., Tinti, E., & Marone, C. (2017). Evolution of shear fabric in granular fault gouge from stable sliding to stick slip and implications for fault slip mode. *Geology*, *45*(8), 731–734. doi: 10.1130/G39033.1

Sibson, R. H. (1996). Structural permeability of fluid-driven fault-fracture meshes. *Journal of Structural Geology*. doi: 10.1016/0191-8141(96)00032-6

Sibson, R. H. (1998). Brittle failure mode plots for compressional and extensional tectonic regimes. *Journal of Structural Geology*. doi: 10.1016/S0191-8141(98)00116-3

Skarbek, R. M., Rempel, A. W., & Schmidt, D. A. (2012). Geologic heterogeneity can produce aseismic slip transients. *Geophysical Research Letters*, *39*(21), 1–5. doi: 10.1029/2012GL053762

Ujiie, K., Saishu, H., & Fagereng, Å. (2018). An Explanation of Episodic Tremor and Slow Slip Constrained by Crack-Seal Veins and Viscous Shear in Subduction Mélange. , 1–9. doi: 10.1029/2018GL078374

van Dinther, Y., Gerya, T. V., Dalguer, L. A., Mai, P. M., Morra, G., & Giardini, D. (2013). The seismic cycle at subduction thrusts: Insights from seismo-thermo- mechanical models. *Journal of Geophysical Research: Solid Earth*. doi: 10.1002/2013JB010380

Wallace, L. M., & Beavan, J. (2010). Diverse slow slip behavior at the Hikurangi subduction margin, New Zealand. *Journal of Geophysical Research: Solid Earth*, *115*(12), 1–20. doi: 10.1029/2010JB007717

Wassmann, S., & Stöckhert, B. (2013). *Rheology of the plate interface - Dissolution precipitation creep in high pressure metamorphic rocks.* doi: 10.1016/j

.tecto.2013.09.030

Webber, S., Ellis, S., & Fagereng, Å. (2018). Virtual shear box experiments of stress and slip cycling within a subduction interface mélange. *Earth and Planetary Science Letters*. doi: 10.1016/j.epsl.2018.01.035